대용량 광신호 연결을 위한 평판 마이크로 광학계

Planar microoptics for massively parallel optical interconnections

송 석 호
한국전자통신연구소 기초기술연구부
대전시 유성우체국 사서함 106, (우)305-600
(tel)042-860-5556 (fax)042-860-5033 (email)shsong@utopia.etri.re.kr

For massively parallel optical interconnections, we propose three types of planar optical configurations for crossover photonic switching network, backboard optical signal distribution, and high speed packet address detection. The planar overlays allow 2-D pixel arrays located on a wafer scale integrated circuit to be interconnected in a compact and vibrationally robust configuration. By the laser writing technique surface relief profiles of microoptical Fresnel lenses and multiplex gratings used in the planar optics are successfully fabricated.

I. Introduction

Planar optical systems, which consist of free-space optical components integrated on a single substrate, have been developed by using planar fabrication techniques of microelectronic or optoelectronic circuits. It is known that the planar optics does not suffer from problems of the alignment of many components and the mechanical instability, as well as it maintains a high connectivity of the free-space optics[1]. In the free-space optics a complicated mechanical alignment is required to arrange the components to within several micrometer accuracy, and this is a common problem in most approaches of the free-space optical implementation of regular interconnection networks as well. To overcome this alignment complexity, interest in the planar optics approach has grown recently.

Planar optical systems contain bulk optical components integrated on a single substrate. Lithographic fabrication techniques can be used to form the various optical elements (diffractive-reflective holograms, microlenses, microprisms, etc), and optoelectronic elements (modulators, detectors, etc) on a single side of the substrate. This has the advantages that they can be accurately aligned using one mask set to give a mechanically robust interconnect and the fabrication technique is compatible with microelectronic circuits. Many types of the planar optics have been developed so far, to implement clock signal distributions in an optoelectronic circuit board[2], 1-to-1 connections (space-invariant imaging)[3], and N-to-N connections (space-variant imaging)[4].

In section II, we describe a planar optical configuration to implement crossover switching interconnects. The concept of planar optics is implemented to a backboard optical signal distribution in section III, and to a high speed packet address detection in section IV. Finally, the laser writing technique is introduced to fabricate several types of planar microoptic components in section V.

II. Planar microoptical interconnects for crossover photonic switching

Switching networks, such as crossover, perfect shuffle, and Banyan, are being widely considered for use in regular multistage interconnection topologies for telecommunications and in

multiprocessor computers for shared memory access, because of their simplicity, extendibility, and high throughput[5]. The free-space optical crossover interconnect developed by Bell Labs[6] would be one of the promising results for optical switching networks. In this section, we present a planar optical implementation of the crossover interconnect integrated onto a compact solid optical substrate.[7]

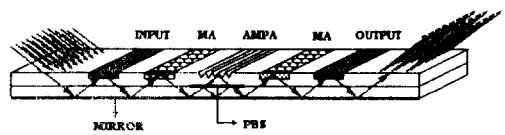

Figure 1. Planar optic design of 3-dim. crossover interconnects.

The planar optical crossover interconnects is shown in Fig.1, where only one of the multiple layered crossover interconnection stages is illustrated. The configuration consists of a switching node array (input stage) of a 2-D optical logic device array, connected via a 4-f imaging system to the acute-angle microprism array(MA), and then via a further 4-f imaging system to the second switching node array (output stage). Two optical substrates are glued together and the polarizing beam splitter(PBS) is located in between them. The PBS splits each input beam into a pair of bypass- and cross-connections and recombines them into one. Two lens arrays, MA, and optoelectronic devices of INPUT/OUTPUT are designed on the top surface, while a mirror layer is under the bottom surface. They can be lithographically fabricated with a very accurate alignment. For the microlenses, refractive microlens[8] or Fresnel-type diffractive microlens with multiple phase levels[9], would be used. The use of a silicon substrate offers the potential for integrating both the optoelectronic devices and their driving electronics with the optical components, all on the same substrate, and it would also be attractive for integrating liquid crystal devices to control the polarization of signal beams.

For demonstration of the planar optical crossover interconnections, we have used the MA fabricated using standard silicon V-grooves technology[10]. Figure 2(a) shows the SEM photograph of the MA fabricated on a silicon wafer. The apex-angle of the prism is 70.52 degrees and the base width of each prism is 128 μm. In the experiment, we implemented only the cross-connections by using discrete optical components; an input mask, two lenses, and the MA described above. The input was imaged to the MA via a lens and the cross-connected output was then imaged to a screen via the other lens. The angles of incidence and reflection at the MA were about 20 degree. The input mask shown in Fig.2(b) consists of transparent and opaque pixels arranged in a 8x8 array format with each pixel having a diameter of 30μm. We designed the dark field input pattern as an "X" shape by making the corresponding pixels transparent, and in this case 4 transparent pixels fall within any single 128μm column width as shown in Fig.2(b). Figure 2(c) shows the cross-connected output of the experiment. At the corresponding microprism, each set of the four pixels in the input mask are flipped horizontally.

Therefore, the experimental result gives us a possibility for the implementation of a planar optical crossover interconnection with 3-D spatially parallel connectivity.

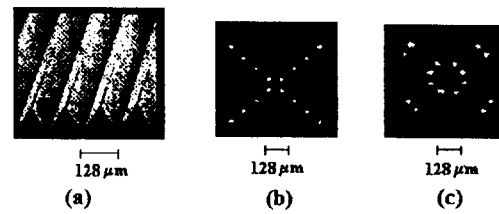

Figure 2. Experimental result of crossover interconnects. (a) Acute-angle microprisms, (b) input with 30μm pixels, (c) output.

Interconnection capacity of the planar integrated optics for the crossover network can be analyzed by considering two micro-optical configurations on the base of Gaussian beams being relayed by

microlens arrays[11], as shown in Fig. 3. They correspond to two possible optical configurations for collimating Gaussian beams with Z_1=f (represented as type-A) shown in Fig. 3(a) and Z_1=f+Z_R (type-B) shown in Fig. 3(b), where Z_1 is given by the path length from an input to the microlens array with the focal length of f, and the Rayleigh range of Z_R. Diameter of the microlenses, d_L, and the path length from the lenses to the position where the minimum beam waist takes place after a beam passes through the lenses, Z_2, are given by,

$$d_L = 2kw_o\left[1+\left(\frac{Z_1}{Z_R}\right)^2\right]^{1/2}, \qquad (1)$$

$$Z_2 = f_{A,B} + \frac{f_{A,B}^2(Z_1 - f_{A,B})}{(Z_1 - f_{A,B})^2 + Z_R^2}, \qquad (2)$$

where, ω_o is the input beam waist, and k the clipping ratio defined by the ratio of d_L to $2\omega_o$.

If we assume that both the width of AMPA and the separation distance between the microlens array and the AMPA are equal to the width of the microlens array, the interconnection capacity of the type-A, N_A, can be derived with the help of Eq.(1) and (2) as follows:

$$N_A = \frac{Z_2}{2d_L}\cos\theta$$

$$= \frac{\pi n\omega_o^2\cos\theta}{2\lambda d_L}\left[\left(\frac{d_L}{2k\omega_o}\right)^2 - 1\right]^{1/2}, \qquad (3)$$

where, θ is the angle between the incident beam and the mirror plane, and n is the refractive index of the substrate. For several d_L of 120μm, 240μm, 480μm, and 960μm, Fig.3(c) shows a plot of Eq.(3) as a function of ω_o, when the clipping ratio of k=1.52, λ=850nm, n=1.5, and θ=45 degrees. The N_A increases with the d_L, but it has a maximum value at a certain ω_o. The interconnection capacity of the type-B, N_B, can be also obtained by

$$N_B = \frac{Z_2}{2d_L}\cos\theta$$

$$= \frac{\pi n\omega_o^2\cos\theta}{4\lambda d_L}\left[\left(\frac{d_L}{2k\omega_o}\right)^2 - 2\right], \qquad (4)$$

and it is plotted in Fig.3(d) by the solid curves against ω_o. The dashed line in this figure represents the constraint of Z_2=2Z_1. The four corresponding intersections of the solid and dashed lines show the maximum number of channels of the type-B configuration at the given d_L, respectively. Each of the solid curves reveals a decreasing behavior as the ω_o increases, and it is distinctly different from that of the Type-A. It is because, if $d_L >> \omega_o$, the N_A of Eq.(3) is proportional to ω_o, while the N_B of Eq.(4) does not strongly depend on ω_o and it slightly decreases as the ω_o grows. The constraint of Z_2=2Z_1 in the Type-B configuration makes a severe restriction to design a planar crossover interconnect. Therefore, we can conclude that the type-A configuration with the relation of Z_1=Z_2 =f_A can be more flexible to choose the diameter of microlenses for a given ω_o, and it can have an interconnection capacity greater than the type-B.

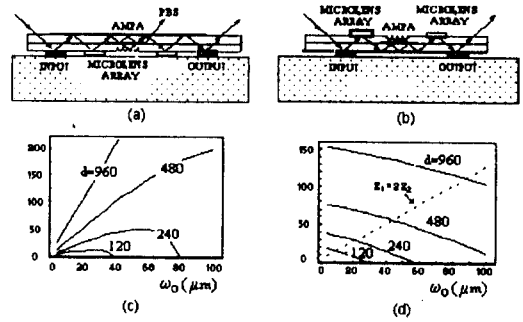

Figure 3. (a)Type-A and (b)type-B planar optical configurations for crossover interconnects. Interconnection capacities of (c)type-A and (d)type-B.

III. Backboard optical interconnect using focusing grating coupler arrays in a planar optics

Backboard interconnections are widely used for distribution of common input signals to several processing boards, and they are considered as one of the most attractive fields to which the optical interconnection technology can be applied[12]. Efficient connections between the backboard interconnect and I/O ports should be taken into consideration in the design of backboard interconnections. Generally the number of data transmission lines in the backboard interconnects is less than a hundred, and each data line delivers single instruction to all boards at a given time slot. Therefore, it could be more acceptable to make the I/O ports in an 1-D array format rather than in a 2-D array. The use of 1-D I/O ports allows one to implement an efficient interconnection, since one may transmit high-speed signals by means of well-developed techniques by using fibers and waveguides, and by connecting fibers to waveguides[13].

We have designed a 1-D array of focusing grating couplers(FGC) in a backboard interconnection scheme which consists of 1-D fiber arrays as the I/O ports and a slab waveguide as the backboard interconnect[14]. In order to make a highly uniform distribution of optical signals to several processing boards, two design parameters of the FGC length and duty cycle of square gratings in a FGC, have been evaluated. The design of the FGC arrays is based on the ray-optic concept[15] for propagation-mode analysis in a slab waveguide, and the rigorous coupled-wave theory[16] has been used to calculate the out-coupling efficiency of radiation-modes. It has been found that the backboard interconnection scheme incorporating the 1-D FGC arrays, when used to distribute a guided optical power of TE_0-mode to several converging waves radiated only toward a glass substrate, displayed a power uniformity of 5% and a total coupling efficiency of 95%, which can be highly acceptable in practical use.

Figure 4(a) is an illustration of the backboard interconnection scheme incorporating several 1-D arrays of FGC's proposed here. It consists of optoelectronic integrated circuit (OEIC) boards mounted on a glass substrate, a slab waveguide with an absorption layer on the one edge, 1-D arrays of FGC's on the bottom surface of the waveguide layer, butt-coupled fibers for input signals, and waveguide lenses for collimating the guided waves. It is assumed that the waveguide is designed only for a TE_0 mode. As shown in Fig. 4(b), the input signal beams guided into the slab waveguide are collimated by the waveguide lenses, and they propagate in the direction of y-axis. Each of the collimated guided-waves is then out-coupled by a 1-D array of N(=5 in the figure) FGC's, resulting into several diffraction waves as radiation-modes focused onto the photodiodes as depicted in Fig. 4(c). Therefore, each of 1-D arrays with N FGC's produces N converging waves.

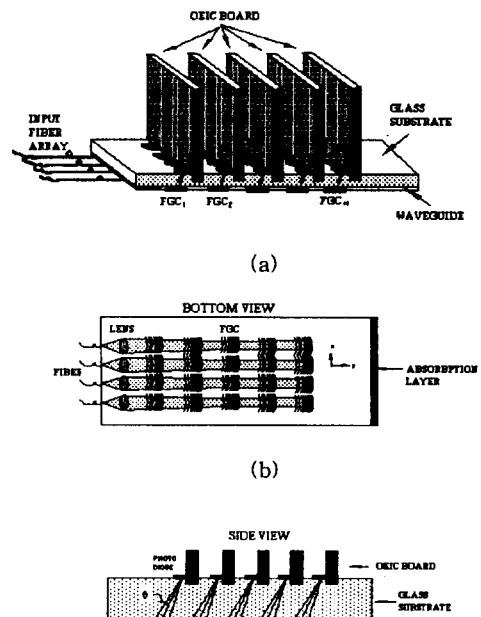

Figure 4. Backboard interconnection scheme with 1-D array of FGC's. (a)3-D view, (b)bottom view, and (c)side view.

A FGC in the Fig. 4 can be described by the following equation:

$$y=\frac{1}{(N^2-n_s^2)}\left(m\lambda N+Nn_sf-n_s^2f\sin\theta-n_s\sqrt{A}\right),$$
$$A=(N^2-n_s^2)x^2+m^2\lambda^2+2m\lambda f\,(n_s^2-N\sin\theta)+f^2(N-n_s^2\sin\theta)^2,$$
$$m=0,\pm1,\pm2,\ \ldots \qquad (5)$$

where n_s is the refractive index of glass substrate, N is the effective index for a guided mode, λ is the wavelength in vacuum, f is the focal length of FGC's, and θ is the diffraction angle. The spatial frequency and the direction of the gratings vary across the grating area so that the guided light is diffracted at each point of the chirped grating toward the focal point with the diffraction angle of θ.

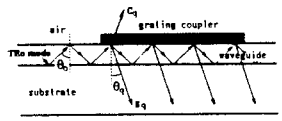

(a)

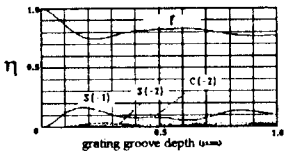

(b)

Figure 5. (a) Ray-optic concept for radiation-mode analysis and (b) diffraction efficiency of a square grating profile in FGC's.

Figure 5(a) shows the ray-optic concept to analyze propagation-modes in a slab waveguide. The propagation angle of TE_0-mode is θ_0, the effective index $N = n_f \sin\theta_0$, and the effective thickness T_{eff}. Λ is the grating period, and D is the duty cycle defined by the ratio of grating medium length to Λ. According to the ray-optic concept, we can consider the out-coupling of TE_0-mode from the FGC as multiple diffraction of the ray bouncing inside the waveguide medium with an angle of θ_0. The number of bounces, M, from the FGC layer are given by

$$M=\frac{L}{2T_{eff}\tan\theta_o}, \qquad (6)$$

where L is the length of FGC. The guided wave is diffracted M-times both to the substrate and air. In the Fig.5, the diffraction efficiency of the q-th order substrate-mode and air-mode of radiated waves are defined by S_q and C_q, respectively, where t defines the efficiency of zeroth order diffraction.

The diffraction efficiencies of S_q, C_q, and t, have been calculated by the rigorous coupled-wave theory, and the results are shown in Fig. 5(b) as a function of the grating groove depth. In the calculation, the FGC with a square-shaped grating was estimated with the parameters of D=0.5, n_s=1.46(quartz glass), n_f=1.52(ThF_4), n_g=1.49(PMMA), n_o=1.0(air), λ=633nm, T_s=3mm, T_f=1.0μm for guiding only a TE_0 mode, T_{eff}=1.38μm, N=1.62, θ_0=80.7 degree, Λ=2.14λ, and θ_{-1}=45 degree. The focal length, f, of the FGC was $T_s/\cos\theta_0$. Most of the diffraction efficiencies of substrate-modes and air-modes are lower than 20%, since the relation of Λ and θ_0 are out of Bragg condition. In the range of the groove depth less than 0.1μm, the efficiencies are negligible except for the first-order of substrate-modes, S_{-1}.

After the M times diffraction from a FGC of the length L, the OCE of each radiation-mode can be calculated by

$$\eta_{i,q}^{tot}=i_q+i_qt+i_qt^2+\ldots+i_qt^{(M+1)}=i_q\frac{(1-t^M)}{(1-t)}, \qquad (7)$$

where, i=C for air modes and i=S for substrate modes, and the optical power remaining in the waveguide is given by t^M, for the incidence of unit optical power.

In order to get a uniform distribution, the OCE's, η_1, η_2, ..., and η_N, of the FGC's must keep the relation of

$$\eta_n = \frac{\eta_1}{[1-(n-1)\eta_1]}, \quad n=1, 2, \ldots, N. \quad (8)$$

By equating η_n to the OCE of Eq.(7), we can obtain an optimized length of each FGC for the uniform power distribution as follow.

$$L_n = \frac{1}{2\alpha_r} \ln \frac{S_{-1}}{[S_{-1}-(1-t)\eta_n]}, \quad (9)$$

$$\alpha_r = -\frac{M}{2L} \ln(t).$$

An example of our design results is shown in Fig. 6, when N=10 and the grating groove depth is 50nm. The 10 dots in the figure represent the designed length L, and duty cycle D, of each FGC. In order to make the spot size focused on the photodiodes smaller than the size of detection windows, L must be large enough, so that in the example we chose the length in the range from 180mm to 500mm. The first 7 FGC's have D=0.9, the 8-th and 9-th FGC's have D=0.8, and the last FGC has D=0.5. The OCE of each FGC has a value from η_1 =9.91% up to η_{10}=91.93%, respectively, in accordance with the Eq.(8). The total out-coupling efficiency defined by the ratio of the total optical power coupled out of the 10 FGC's to the incident power, is therefore 99.1%.

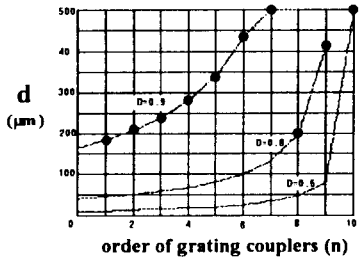

Figure 6. Design result of the lengths and the duty cycles of ten FGC's for a uniform power distribution.

IV. Planar optical interconnections for 100Gb/s packet address detection

Interests in optical packet switching networks have been ever increasing to fully utilize the enormous bandwidth of optics in order to satisfy the bandwidth requirements for future broadband multimedia communications. In packet (or cell) based optical switching networks[17], a header attached to each packet payload contains a destination address to route the payload to the proper destination. Since the speed of header detection process at each switching node affects the network throughput significantly, optical means have been sought to improve the header detection speed. The header processing schemes proposed so far are mainly based on fiber-optic loop-mirror configurations[18] and fiber-optic correlators[19]. Even though they utilize the enormous bandwidth of optical fibers in order to satisfy the bandwidth requirements for future broadband multimedia communications, they may suffer from a large amount of optical loss higher than 12dB due to a series of several 2x2 directional couplers.

In order to reduce the optical loss, we propose a novel scheme of 3-dimensionally integrated planar optics for 100Gb/s packet address detection[20]. The planar optics consists of an array of waveguide grating couplers and a diffractive microlens fabricated on a surface of glass block, and makes it possible to connect 100Gb/s, 10-bits packet address signals to a detector with an efficiency higher than 70%. Therefore, we believe that the planar optics scheme can show much improvement in power requirement, signal processing speed, and component size. For a highly uniform coupling of each optical bit-signals to the detector, structures of the waveguide grating couplers are evaluated by the same approach using the ray-optic concept and the rigorous coupled-wave theory as discussed in the section III.

Figure 7 shows a schematic illustration of the 3-dimensionally integrated planar optics for 100Gb/s packet address detection. It consists of a glass substrate, a butt-coupled fiber for input

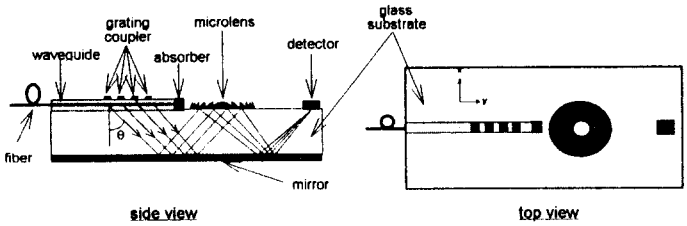

Figure 7. Planar optical scheme for packet address detection.

signals, a waveguide layer with an absorption layer on the one edge, grating couplers(GC) on the top of the waveguide layer, a detector, a diffractive microlens to focus the radiated beams from grating couplers to the detector, and a mirror layer under the bottom surface of the glass substrate. As shown in Fig. 8, one of the GC's consists of line-shape gratings with the grating period of P, the grating thickness of t, and the width of d. The duty-cycle of gratings is defined by g/P.

The signal flow is as follows. The input beams of optical packet signals are guided into the waveguide, and propagate in the direction of y-axis. Each of the guided bit-signals is then out-coupled, with an angle of θ, by the linear array of N(=4 in the figure) GC's, resulting into N diffraction waves as radiation-modes. The diffraction waves are then focused onto the detector by the diffractive microlens. Output characteristics of the packet address detection process can be described as

$$r(t) = \int_0^d \rho\ s(y) f(t-y)\,dy \qquad (10)$$

where ρ is the focusing efficiency of the microlens, s(y) is an incoming packet address signal and f(y) is the impulse response function of the GC. If the incoming packet address is in a digital form with bit-interval of τ, s(y) with N address-bits and f(y) are expressed by

$$s(y) = \sum_{i=1}^{N} W_i A_i(y), \qquad)$$

$$f(y) = \sum_{j=1}^{N} \eta_j\ rect(y/\Delta y_j) * \delta(y-y_j), \qquad (12)$$

where Wi and $A_i(y)$ are the weighting factor and waveform of the i-th address bit, respectively. In Eq. (12), * denotes the convolution and η_j, Δy_j, and $\delta(y-y_j)$ are the parameters for the j-th GC describing respectively the out-coupling efficiency, the width, and the delta function representing the center positions. If the code sequences of s(y) and f(y) are identical, the GC's generates an output of auto-correlation delta peaks. Otherwise, the filter generates cross-correlation peaks. As an example, if the s(y) is represented by the sequence (1011010011) and f(y) by the same sequence (1011010011), then under ideal circumstances the auto-correlation signal would be (1112213226223122111). Since the central peak value, 6, of the auto-correlation signal is always higher than cross-correlation peak values, it can be easily decided whether the address of an incoming optical packet matches to a specific node address stored in the GC's by thresholding the correlation outputs with a level in between two values of the central auto-correlation peak and the highest cross-correlation peak.

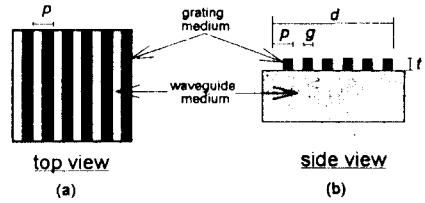

Figure 8. Structure of the grating coupler.

Speed of the packet signal detection is only

limited by the spacing between the GC's. If the spacing is 2mm and the refractive index of the waveguide layer is about 1.5, then the time interval, τ, between the bit-signals is given by 10^{-11} second. Therefore, it is possible to get the detection speed of packet address bit-signals in the range of 100Gb/s. In order to produce higher peak values of the auto-correlation pulses, it is desirable to make the ρ and the sum of η_j for all j to be high. Since the use of a Fresnel-type lens as the diffraction lens can make the ρ to be high, we have fabricated the lens by using the laser writing technique as will be described in the next section. If we assume the total out-coupling efficiency (η_{GC}) of the GC's to be about 90% and the value of 78% reported in experiment as the focusing efficiency ρ of the microlens[21], one can mention that the overall detection efficiency obtained from the grating couplers and the diffractive microlens would be (η_{GC} x ρ) = 70.2%.

V. Laser writing technique

In the fields of optical communication and optoelectronic processing, microoptical interconnections make a potential to improve the degree of system integration and stability. Microoptical components for focusing, imaging, branching, combining, and so on, have progressed beyond prototypes by the fabrication techniques of PR melting, ion exchange, deposition, e-beam writing, and laser writing.[22] The writing technique using e-beam or laser beam makes it possible to produce an arbitrary surface profile, such as the continuous surface-relief grating for spot array generators or a set of diffractive and/or refractive components on a same substrate[23]. In this section, the laser writing technique is described and fabrication results of the Fresnel-type microlens and the computer generated hologram (CGH) for a pattern generation are presented.

The Fresnel-type microlens is represented by the following phase profile:

$$\phi(x,y)=\frac{2\pi(n_s-n_o)}{\lambda}\times\{\sqrt{x^2+y^2+f^2-2yf\sin\theta}-f\}-2\pi m,$$

$$m=0,\ 1,\ 2,\ \ldots \qquad (13)$$

Since the phase has a continuous value from zero to 2π, it may not be possible to fabricate the continuous structure by the lithographic technique used in general. Therefore we have developed the laser writing system, and its schematic diagram is shown in Fig. 9.

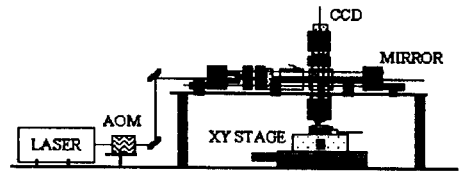

Figure 9. Laser writing system.

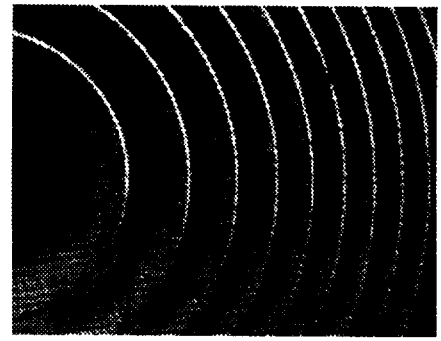

Figure 10. Fresnel microlens fabricated by the laser writing.

The laser writing system consists of air-cooled Ar^+ laser (λ=458nm), acousto-optic modulator (AOM), XY positioning stage with a moving resolution of 0.1μm, and CCD camera and mirror for monitoring the beam focusing on a sample substrate. The sample substrate of optical glass with a positive photoregist (AZ1400) layer was exposed by the raster-scanned laser beam, and

was developed with the solution of AZ351. Based on the gamma curve of the photoregist layer, any surface-relief micro-structure can be fabricated as it was designed. The spot size of the incident beam focused on the photoregist layer was measured by 2.3㎛.

Figure 10 shows the photograph of a Fresnel-type microlens fabricated by the laser writing. F/# of the lens was 10 and the diameter was 250㎛. It shows us that the continuous surface profile of the Fresnel microlens can be implemented by the laser writing. The very fine horizontal lines in the photograph came from the marks of the laser beam scanning.

Figure 11. Computer-generated hologram fabricated by the laser writing.

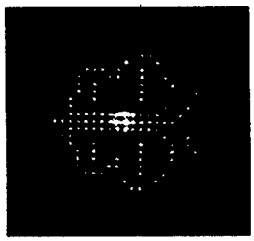

Figure 12. Fourier transform pattern of the CGH shown in Fig. 11.

Figure 11 is the photograph of a CGH fabricated. The CGH consists of four phase levels instead of a continuous phase profile[24], and its minimum pixel size was 1.0㎛. The Fourier transform image of the CGH is shown in Fig. 12. Intensities of the spots are not so uniform, but it can be mentioned that the CGH fabricated by the laser writing system would be enough to generated a spots pattern with a 2-D array format. We expect that a more uniform spot array can be obtained by control of the phase levels more accurately,

VI. Conclusion

As an approach to overcome some practical limits of free-space optics on applications, such as alignment complexity, lack of stability, and difficulty in integration, we have described the 3-dimensional planar optics concept.

Three types of planar optical configurations for crossover photonic switching network, backboard optical signal distribution, and high speed packet address detection have been proposed. Their potentials for massively parallel optical interconnections have been also analyzed.

By the laser writing technique, any microoptical components, even they have continuous surface- relief profiles, can be fabricated on a single substrate within a same process. Therefore it can be mentioned that the laser writing is a very useful technique since it makes possible to fabricate most of all passive components used in a planar optics.

References

1. J. Jahns and A. Huang, Appl. Opt. **28**, 1602 (1989).
2. S. Walker and J. Jahns, Opt. Comm. **90**, 359 (1992)
3. J. Jahns and B. Acklin, Opt. Lett. **18**, 1594 (1993).
4. S. Song, C. Carey, D. Selviah, and J. Midwinter, Appl. Opt. **32**, 5022 (1993).
5. D. Agrawal, IEEE Trans. Computer, **C-32**, 637 (1983).
6. J. Jahns and M. Murdocca, Appl. Opt. **27**, 3155 (1988).
7. S. Song, E. Lee, C. Carey, D. Selviah, and J. Midwinter, Opt. Lett. **17**, 1253 (1992).

8. J. Leggatt and M. Hutley, Electron. Lett. **27**, 238 (1991).
9. J. Jahns and S. Walker, Appl. Opt. **29**, 931 (1990).
10. K. Petersen, Proc. IEEE, **70**, 20 (1982).
11. F. McCormick, F. Tooley, T. Cloonan, J. Sasian, and H. Hinton, Opt. Quantum Electron. **24**, S465 (1992).
12. K. Rastani and W. Hubbard, Appl. Opt. **31**, 4863 (1992).
13. W. Hunziker, W. Vogt, and H. Melchior, in Integrated Photonics Research, vol.3 of 1994 OSA Tech. Digest Series (OSA, 1994), paper SaC3.
14. S. Song and E. Lee, to be published at Appl. Opt. 10 July, 1995.
15. H. Kogelnik, *"Theory of dielectric waveguide", in Integrated Optics*, T. Tamir, ed. (Springer-Verlag, Berlin, 1975), pp15-29.
16. M. Moharam and T. Gaylord, J. OSA, 72, 1385 (1982).
17. R. Fortenberry, Y. Cai, and R. Tucker, OFC/IOOC '93 Tech. Digest, 1993, pp21-22.
18. I. Glesk, J. Sokoloff, and P. Prucnal, Electron. Lett. **30**, 1322 (1994).
19. P. Prucnal, D. Blumenthal, and P. Perrier, Opt. Eng. **26**, 473 (1987).
20. S. Song and E. Lee, to be published at Proc. of *2nd Inter. Conf. on Massively Parallel Processing Using Opt. Interconn.* Oct. 23-24, 1995, San Antonio, Texas, USA.
21. T. Shiono and H. Ogawa, Appl. Opt. **30**, 3643 (1991).
22. M. Gale, M. Rossi, J. Pedersen, and H. Schutz, Opt. Eng, **33**, 3556 (1994).
23. M. Hutley, *Microlens Array* (Inst. of Physics, Reading, UK, 1991).
24. M. Dames, R. Dowling, P. McKee, and D. Wood, Appl. Opt. **30**, 2685 (1991).